ACS APPLIED MATERIALS & INTERFACES
Research Article
www.acsami.org

High-Performance Dispenser Printed MA p-Type $Bi_{0.5}Sb_{1.5}Te_3$ Flexible Thermoelectric Generators for Powering Wireless Sensor Networks

Deepa Madan,[†,*] Zuoqian Wang,[†] Alic Chen,[†] Paul K. Wright,[†] and James W. Evans[‡]

[†]Department of Mechanical Engineering and [‡]Department of Materials Science and Engineering, University of California, Berkeley, California 94720, United States

ABSTRACT: This work presents a novel method to synthesize p-type composite thermoelectric materials to print scalable thermoelectric generator (TEG) devices in a cost-effective way. A maximum *ZT* of 0.2 was achieved for mechanically alloyed (MA) p-type $Bi_{0.5}Sb_{1.5}Te_3$ (8 wt % extra Te additive)-epoxy composite films cured at 250 °C. A 50% increase in Seebeck coefficient as a result of adding 8 wt % extra Te in stoichiometric $Bi_{0.5}Sb_{1.5}Te_3$ contributed to the increase in *ZT*. To demonstrate cost-effective and scalable manufacturing, we fabricated a sixty element thermoelectric generator prototype with 5.0 mm × 600 μm × 120 μm printed dimensions on a custom designed polyimide substrate with thick metal contacts. The prototype TEG device produced a power output of 20.5 μW at 0.15 mA and 130 mV for a temperature difference of 20 K resulting in a device areal power density of 152 $\mu W/cm^2$. This power is sufficient for low power applications such as wireless sensor network (WSN) devices.

KEYWORDS: *printed electronics, $Bi_{0.5}Sb_{1.5}Te_3$ epoxy composites, mechanical alloy, thermoelectric generators, flexible substrate*

INTRODUCTION

A significant amount of heat is wasted to the environment in applications such as heat engines; car exhausts and pipes carrying hot fluid. Thermoelectric generators can potentially be used to generate electricity from this low-grade waste heat and play an important role in powering the condition monitoring sensors around engines, motors, pipes, etc.[1] However, performance of these devices depends on both materials properties and device geometry[2,3] and their efficiency is low.[4] The efficiency of TEG is governed by the dimensionless figure of merit, *ZT*. It has been challenging to increase *ZT* beyond 1.5 for commercial thermoelectric materials like Bi_2Te_3 as n-type material and $Bi_{0.5}Sb_{1.5}Te_3$ as p-type material, because the thermoelectric parameters of *ZT* are generally interdependent.[5] There are challenges on the device design side as well. The electrical resistance and the temperature difference across the device depend on the element length of the device. Electrical resistance increases with increase in element length resulting in lower power output. Temperature difference across the device increases with increase in element length resulting in higher power output. Therefore, a trade-off occurs between an application specific optimized device length and power output.

WSNs are a promising technology for ubiquitous, active monitoring in residential, industrial and medical applications. A current bottleneck for widespread adoption of WSN's is the power supplies. Although the power demands can be somewhat alleviated through novel electronics, any primary battery will have a finite lifetime. This can pose a major problem if the network is large or the nodes are located in difficult to reach areas. Replacement of these batteries may be tedious and expensive. Thermal energy is an attractive option to power WSNs due to the availability of low-grade ambient waste heat sources.To be used for powering the WSNs, the TEG should be able to provide power at certain desired voltage levels.[6] A high voltage output requires large number of couples packed in a small area in addition to high Seebeck coefficient and high temperature difference across the device.[7]

Devices utilizing waste heat to generate power should be low cost. Conventional manufacturing techniques for TEG devices require extensive usage of labor, materials and energy.[4] The alternative microfabrication technology involves expensive and complicated processes. We utilize direct-write printing technique to fabricate microscale TEGs. Printing is an additive and cost-effective method for fabricating thick film structures. It is an automated process that can be used to print high-aspect-ratio devices with minimum labor. High cost micro fabrication steps such as etching and thin film deposition became redundant with the use of printing. It is easy to automate printing process that requires minimal labor in scaled manufacturing and the reduction of manufacturing costs associated with printing is significant.[8,9]

Printing of high-aspect-ratio TEG devices requires thermoelectric materials that are readily synthesized, air stable, and a solution process able to create patterns on large areas. In this regard, polymer thermoelectric composites are very attractive, as they require relatively simple manufacturing processes.[10,11]

Received: August 23, 2013
Accepted: October 25, 2013
Published: October 25, 2013

 © 2013 American Chemical Society dx.doi.org/10.1021/am403568t | ACS Appl. Mater. Interfaces 2013, 5, 11872−11876

However, the ZT of polymer based composite material is very low. In this work, we use a custom developed dispenser printer to print high-aspect-ratio planar single-element TEGs.[12−14] $Bi_{0.5}Sb_{1.5}Te_3$ was chosen as the starting p-type thermoelectric material because of its high ZT value at room temperature.[15,16] This work focuses on optimizing the synthesis and processing parameters to maximize the ZT of $Bi_{0.5}Sb_{1.5}Te_3$-epoxy thermoelectric composites thick films by using Te as an additive. For p-type $Bi_{0.5}Sb_{1.5}Te_3$ alloys, it is well-known that holes are created by the antistructure defects generated by the occupation of Te sites with Bi and Sb atoms.[17] Te as an additive helps to reduce the carrier concentration and improve Seebeck coefficient by inhibiting the formation of antistructure defects during mechanical alloying.[18,19] Additionally, we demonstrate device fabrication techniques for high-density arrays of high-aspect-ratio planar TEGs via a cost-effective, scalable, energy-efficient dispenser printing method.

■ EXPERIMENTAL SECTION

To produce $Bi_{0.5}Sb_{1.5}Te_3$ particles, chunks (1−12 mm size) of elemental bismuth, antimony, and tellurium were mechanically alloyed in the molar ratio.[20] A high-energy planetary ball-mill (Torrey Hills ND 0.4L) was used for mechanical alloying. To improve the thermoelectric properties of the MA $Bi_{0.5}Sb_{1.5}Te_3$, varying amounts of Te (2−10 wt %) was used as a dopant.[4,21] In addition to mechanical alloying, wet grinding was used to reduce the average particle size to 10 μm.[22,23] Thermoelectric composite inks were made using $Bi_{0.5}Sb_{1.5}Te_3$ as active particles and commercial epoxy resin as polymer matrix.[22] Vortex mixer and an ultrasonic bath were used to disperse the particles and mix the active particles in polymer to form well dispersed slurries. 100−120 μm thick composite films were then printed on glass substrates using dispenser printer, and cured at 250 °C for 12 h to form thick films for measuring thermoelectric properties.[4,20,23]

■ DEVICE FABRICATION

Although the device geometry of a TEG depends on application, high density and high aspect ratio are highly desirable for various low waste heat applications.[3,24] A 60 leg planar TEG was dispenser printed on flexible substrate fabricated by Rigiflex Technology Inc.[23] The planar thermoelectric device was fabricated from dispenser printed MA p-type $Bi_{0.5}Sb_{1.5}Te_3$ with 8 wt % extra Te polymer composites slurries. The printed TEG device was cured in argon/vacuum oven at 250 °C. Electrical connections were made using silver epoxy and electrical wires. The illustration and an image of the actual device are shown in Figure 1. Prototype device testing was done using custom test set up within 24 h of curing.[23]

■ RESULTS AND DISCUSSION

The XRD was performed on MA $Bi_{0.5}Sb_{1.5}Te_3$ and MA $Bi_{0.5}Sb_{1.5}Te_3$ with 8 wt % extra Te powder using a Siemens (D5000) X-ray generator using monochromatized CuKα (λ = 1.5418 Å) radiation. The XRD peaks for both graphs are consistent with standard pattern of $Bi_{0.5}Sb_{1.5}Te_3$ (JCPDS49−1713), confirming the formation of MA $Bi_{0.5}Sb_{1.5}Te_3$ as shown in Figure 2. The rhombohedral crystal structure of MA $Bi_{0.5}Sb_{1.5}Te_3$ with space group ($R3m$) remains unchanged with the addition of 8 wt % extra Te.[15]

Dispenser printable thermoelectric composite slurries were made by mixing MA $Bi_{0.5}Sb_{1.5}Te_3$ p-type active material in epoxy resin polymer binder, which is well-known and off the shelf available electrically conductive adhesives.[25] To form a conductive path in composite systems, the volume fraction of conductive active particles in polymer matrix should be higher

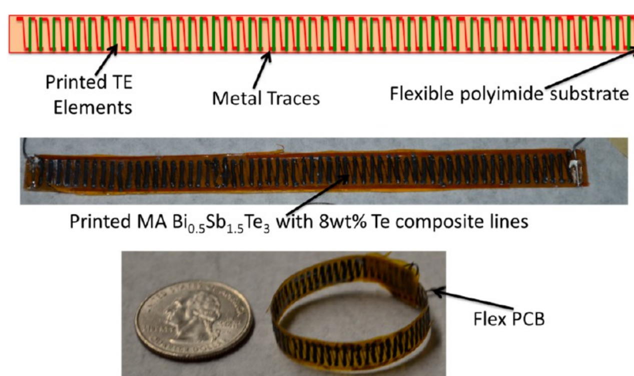

Figure 1. Illustration and image of dispenser printed MA $Bi_{0.5}Sb_{1.5}Te_3$ (with 8 wt % extra Te) p-type planar thermoelectric device on flex PCB substrate.

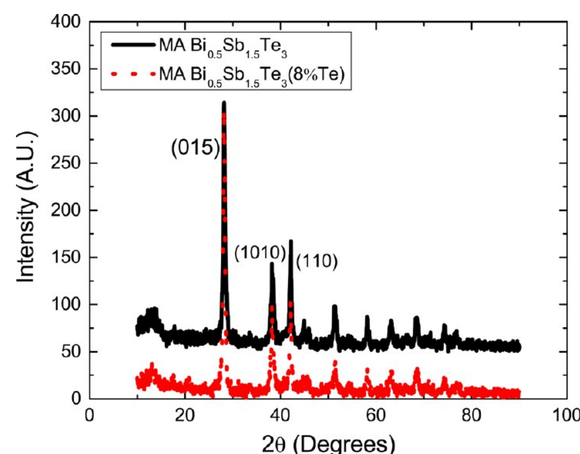

Figure 2. X-ray powder diffraction (XRD) patterns of MA $Bi_{0.5}Sb_{1.5}Te_3$ and MA $Bi_{0.5}Sb_{1.5}Te_3$ with 8 wt % extra Te thermoelectric powders.

than percolation threshold.[26,27] Empirical studies, in this case, show that filler particles to epoxy volume ratio should be 45−55% in order to form the conductive paths. The highest volume ratio of active particles to polymer achieved was 48−52%, beyond which crack formation was observed in the cured film. This higher volume ratio resulted in compact films with minimal cure shrinkage and overall good thermoelectric properties.

Thermoelectric composite materials properties are a function of the polymer matrix and the active particles. Thermoelectric composite materials should have high electrical conductivity and Seebeck coefficient but low thermal conductivity. The electrical conductivity should be high to allow good carrier transport; Seebeck coefficient should be high to provide sufficient voltage; and thermal conductivity should be low to minimize heat losses. However, given the low electrical conductivity of the polymer binders compared to that of active filler thermoelectric materials, the effective properties of the composite system are expected to be less than desirable. To achieve the preferred conductivity of the thermoelectric composite films, we need to optimize curing temperatures. The shrinkage of the polymer matrix upon curing effectively packs the fillers involved. The curing of dispenser printed films was done in the temperature range of 150 to 350 °C.[22] At curing temperatures of 150 and 200 °C films did not give adequate thermoelectric properties. One possible reason is the

inadequate shrinkage of the polymer matrix upon curing to pack filler particles. Cracking was observed in films cured at or above 300 °C. Therefore, p-type dispenser printed films were cured at 250 °C. The curing was done for 12 h to facilitate annealing with the objective of reducing the defects, and hence the carrier concentration, and improving the Seebeck coefficient.[22] Figure 3 shows scanning electron microscope

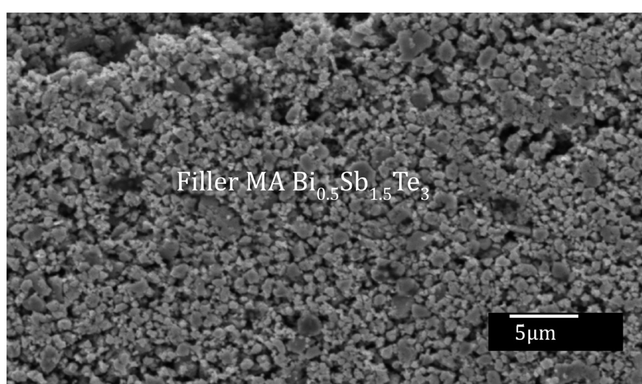

Figure 3. SEM micrograph of MA $Bi_{0.5}Sb_{1.5}Te_3$ p-type filler after wet grinding.

(SEM) image of filler particles after mechanical alloying and wet grinding. From this image, it is clear average particle size is less than 5 μm. Figure 4 shows a cross-section scanning

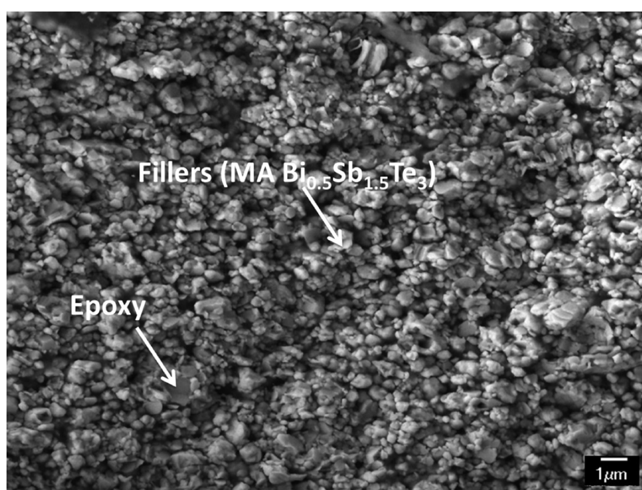

Figure 4. SEM micrograph of dispenser printed MA $Bi_{0.5}Sb_{1.5}Te_3$ p-type composite films cured at 250 °C for 12 h.

electron microscope (SEM) image of a cured $Bi_{0.5}Sb_{1.5}Te_3$/epoxy dispenser printed composite film. The image suggests that the epoxy polymer binder forms a solid, dense matrix when mixed and cured with active $Bi_{0.5}Sb_{1.5}Te_3$ particles. It also suggests that active particles are uniformly distributed in the polymer matrix.

Electrical conductivity and Seebeck coefficient measurement of p-type composite films were done at custom built testing set up. The thermoelectric properties of p-type $Bi_{0.5}Sb_{1.5}Te_3$ thermoelectric composite films cured at 250 °C for 12 h were studied at room temperature and are shown in Figure 5. It is clear from figure 5(a) that dispenser printed MA $Bi_{0.5}Sb_{1.5}Te_3$ composite films have electrical conductivities (12 S/cm) that are 2 orders of magnitude lower as compared to bulk

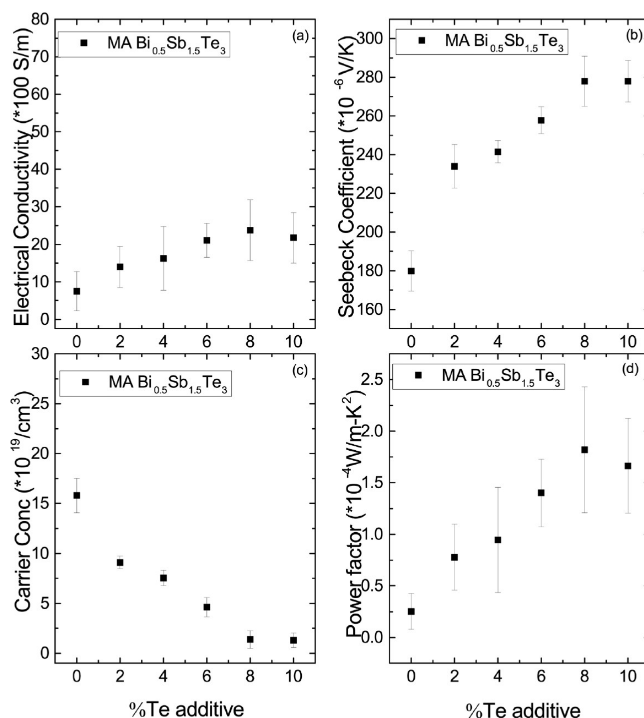

Figure 5. Thermoelectric properties of dispenser printed MA $Bi_{0.5}Sb_{1.5}Te_3$ composite films as a function of extra Te wt% including (a) electrical conductivity, (b) Seebeck coefficient, (c) carrier concentration, and (d) power factor.

$Bi_{0.5}Sb_{1.5}Te_3$ (1300 S/cm).[15] The lower electrical conductivity is due to the nonconducting epoxy polymer matrix.[28−30] The decrease in electrical conductivity may also be due to the grain boundary scattering, which causes carrier mobility to be lower.[23] Addition of Te also did not help to improve electrical conductivity significantly. The slight increase in the electrical conductivity with addition of Te is possibly due to increased grain coalescence facilitated by the presence of extra Te which has lower melting point compared to $Bi_{0.5}Sb_{1.5}Te_3$.[22]

Figure 5b shows Seebeck coefficient variation with respect to Te as an additive. The positive value of the Seebeck coefficient confirms the material as p-type. For stoichometric MA $Bi_{0.5}Sb_{1.5}Te_3$ composite films, the Seebeck coefficient is the same (200 $\mu V/K^1$) as reported for bulk material.[15] According to EMT the Seebeck coefficient of a composite system depend on the effective electrical and thermal conductivity of the composite system. Because electrical conductivity of the insulating polymer is zero, the effective Seebeck coefficient of the composite system is the same as that of MA $Bi_{0.5}Sb_{1.5}Te_3$ and is related to carrier concentration only.[23,30,31] Approximately 50% improvement in the Seebeck coefficient was observed as a result of adding extra Te. Antisite defects are created in the $Bi_{0.5}Sb_{1.5}Te_3$ alloy as Te sites are occupied by Bi and Sb atoms. The hole concentration of p-type $Bi_{0.5}Sb_{1.5}Te_3$ alloy depends on the antisite defects and on the degree of Te-deficiency in the stoichiometric composition.[4,22] Antisite defect concentration decreases with the addition of extra Te as Te-deficiency sites are replaced by extra Te. As a result, the Seebeck coefficient increases.[4] The Hall coefficient and carrier concentration measurements were done using Ecopia-300. Hall effect measurements confirmed slightly lower bulk carrier concentration for films with extra Te, as shown in Figure 5c.

Therefore, the Seebeck coefficient is higher for films with 8 wt % extra Te.

Figure 5(d) shows that the power factor is highest for MA $Bi_{0.5}Sb_{1.5}Te_3$ with 8 wt % extra Te composite films (1.8×10^{-4} W/(m K^2)). Addition of 10% extra Te did not help to improve the thermoelectric materials properties any further. Therefore, we chose MA $Bi_{0.5}Sb_{1.5}Te_3$ with 8 wt % extra Te for making the TEGs. A transient plane source with C-therm TCi thermal conductivity analyzer was used to measure the thermal conductivity. The thermal conductivity of MA $Bi_{0.5}Sb_{1.5}Te_3$ with 8 wt % extra Te dispenser printed film was 0.24 W/(m K). Lower thermal conductivity as compared to the bulk (1.1 W/(m K)) is due to the insulating nature of epoxy. Additionally, fine grain (5 μm) active filler particles increase the potential barrier scattering that also contributes to lower thermal conductivity.[32] A maximum ZT of 0.2 was achieved for dispenser printed MA $Bi_{0.5}Sb_{1.5}Te_3$ with 8 wt %Te composite films.

PRINTED DEVICE PERFORMANCE

To demonstrate the high-energy-density planar prototype, we use MA $Bi_{0.5}Sb_{1.5}Te_3$ with 8 wt % extra Te epoxy-based slurries to print single element on flex PCB board. For demonstration purposes, a nonoptimized planar geometry was chosen. The device resistance of the prototype was 800 Ω when cured at 250 °C. To measure the power output of the device, we attached a variable resistance in series to the device. The maximum power output of the device occurs when the load resistance matches the device resistance as shown in Figure 6.

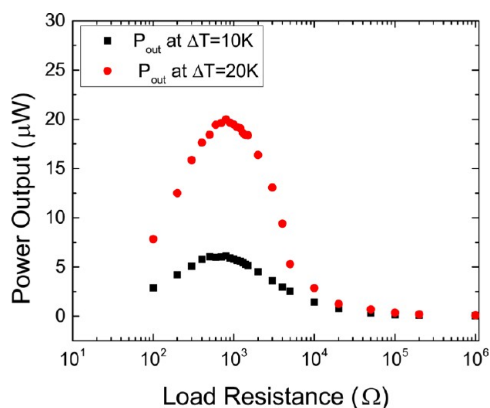

Figure 6. Power output of TEG device as a function of load resistance at ΔT = 10 and 20 K.

Figure 7 shows the device characteristic curve for a sixty-element prototype device measured at ΔT of 10 and 20 K at various load resistances. At matched load resistance, the device produces approximately 20.5 μW at 0.15 mA and 130 mV closed circuit voltages at 20 K temperature difference. Open circuit voltage at 20K temperature difference is 260 mV. At 10 K temperature difference, the maximum power output is 5.5 μW and open circuit voltage obtained is 130 mV. Power output of the thermoelectric device is given by the following equation

$$P_{max} = \frac{V_{op}^2}{4R_{in}}$$

where, $V_{op} = m\alpha\Delta T$and $R_{in} = \rho(l/A)$Where, V_{op} is the open circuit voltage, m the number of couples, α the Seebeck

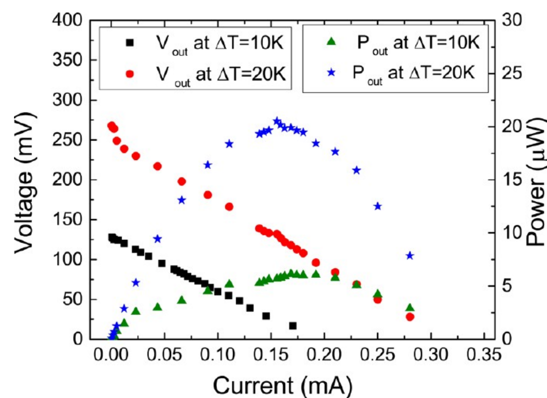

Figure 7. Power output graph of the single thermo-element TEG device at ΔT = 10 and 20 K.

coefficient, and ΔT the temperature difference across the device. R_{in} is the internal resistance of the device; ρ is the electrical resistivity of the composite p-type films; L (5 mm) and A (600 μm × 120 μm) are the length and cross-sectional area of the thermo-element.

The variation in power density (power per unit area) with temperature difference for ideal model, fitted model, and actual measurements of the prototype is plotted in Figure 8. The

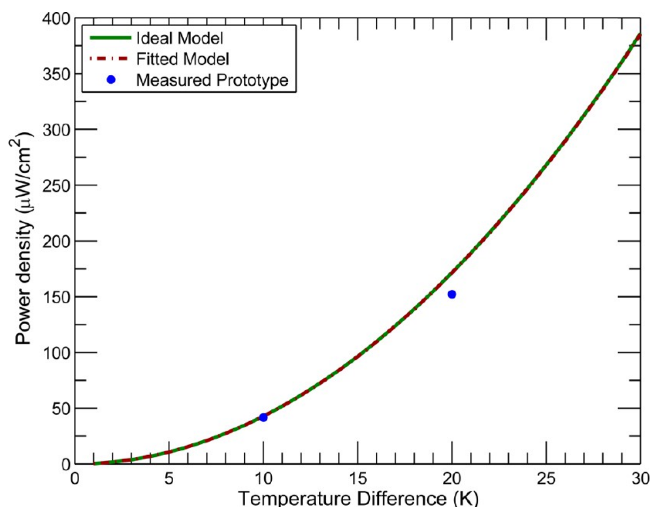

Figure 8. Power density vs temperature difference across the device for ideal model, fitted model, and actual prototype TEG.

power density for the ideal model was calculated using thermoelectric materials properties of MA $Bi_{0.5}Sb_{1.5}Te_3$ with 8 wt % extra Te composites films cured at 250 °C and is shown by solid line in figure 8.[2,3] Figure 8 shows that a maximum power density of 172 μW/cm^2 can be obtained for TEG devices at ΔT (20 K) for the ideal model.

For the fitted model, the power density is calculated based on internal resistance of the device (800 Ω) and Seebeck coefficient of composite films. The power density value for the fitted model and the ideal model matched at ΔT of 10 and 20 K suggesting negligible contact resistance of the TEG device. The actual measured power density values are calculated by dividing the maximum power output of TEG device, produced at ΔT of 10 K and ΔT of 20 K, by the area of the device. It is clear from Figure 8, that a p-type single-element TEG is capable of attaining a power density of 40 μW/cm^2 at

ΔT of 10 K. However, at ΔT of 20 K actual measured power density (152 μW/cm^2) is slightly lower than ideal model (172 μW/cm^2). The graph also indicates that in the higher temperature difference region, power density deviation between ideal model and actual prototype increases. The difficulty in maintaining a high temperature difference across the TEG possibly results in different power densities for the ideal and the actual prototype. Another important thing to notice in Figure 8 is, P_{max} is proportional to $(\Delta T)^2$ as P_{max} depends on the square of the open circuit voltage and the open circuit voltage is proportional to ΔT.

The measurements on the device were repeated after 2 weeks. No significant change in the performance was recorded. However, for many devices a degradation of properties was observed mostly because of the appearance of microcracks in the cured film. Reproducibility and yield of the device are areas that we plan to address in future work.

Printed TEGs are not as efficient as some state-of-the-art TEGs that use high ZT thermoelectric materials. However, the power output results are encouraging for printed TEGs. The power generated by these TEG devices is sufficient to power wireless sensors used in the monitoring of hot surface equipment such as motors, pumps, and steam pipes. The printability of the composite materials allow for a cost-effective, scalable, and high-density fabrication method for TEGs. Although this work demonstrates the feasibility of printed planar TEGs, further application design can be investigated. Future research will include measurements of the power output using TEGs around hot surface equipment generating low-grade waste heat.

CONCLUSIONS

In summary, MA p-type $Bi_{0.5}Sb_{1.5}Te_3$ composite materials were successfully developed for fabricating thermoelectric devices using a dispenser printer. The Seebeck coefficient of MA p-type $Bi_{0.5}Sb_{1.5}Te_3$ was enhanced by adding 8 wt % extra Te. Increase in the Seebeck coefficient and reduction in the thermal conductivity helped to achieve ZT of 0.2. Scalable TEGs were printed on flexible substrate using p-type composite slurries. A maximum power output of 20.5 μW was obtained at 0.15 mA and 130 mV for ΔT of 20K. It resulted in an areal power density of 150 μW/cm^2. This power is suitable for charging the batteries used in wireless sensor networks. These results are encouraging for cost-effective and scalable TEGs that can potentially be used for various low waste heat applications.

AUTHOR INFORMATION

Corresponding Author

*E-mail: deepam@berkeley.edu.

Notes

The authors declare no competing financial interest.

ACKNOWLEDGMENTS

The authors thank the California Energy Commission for supporting this research under contract 500-01-43. We also thank Michael Nill, Jonathan Brown, Brian Mahlstedt, Kevin Huang, and Jay Keist for their contributions.

REFERENCES

(1) Goldsmid, H. J.; Douglas, R. W. *Br. J. Appl. Phys.* **1954**, *5*, 386−390.

(2) Glatz, W.; Muntwyler, S.; Hierold, C. *Sens. Actuators, A* **2006**, *132*, 337−345.

(3) Strasser, M.; Aigner, R.; Lauterbach, C.; Sturm, T. F.; Franosch, M.; Wachutka, G. *Sens. Actuators, A* **2004**, *114*, 362−370.

(4) Rowe, D. M. *CRC Thermoelectrics Handbook*; Taylor and Francis: Boca Raton, FL, 2005; Chapter 46: Micro to Nano.

(5) Majumdar, A. *Science* **2004**, *303*, 777−778.

(6) Koplow, M.; Chen, A.; Steingart, D.; Wright, P. K.; Evans, J. W. *Proceedings of the 5th International Workshop on Wearable and Implantable BSN*; Hong King, June 1−3, 2008 ; IEEE: Piscataway, NJ, 2008.

(7) Chen, A.; Madan, D.; Wright, P. K.; Evans, J. W. *J. Micromech. Microeng.* **2011**, *21*, 104006.

(8) http://ei.haas.berkeley.edu/c2m/pdf/2011EndofYearSlides/ThermoelectricMaterial.pdf Accessed Oct. 6, 2013.

(9) Weber, J.; Potje-Kamloth, K.; Haase, F.; Detemple, P.; Volklein, F. *Sens. Actuators, A* **2006**, *132*, 325−330.

(10) Zhang, B.; Sun, J.; Katz, H.; Fang, F.; Opila, R. L. *ACS Appl. Mater. Interfaces* **2010**, *2*, 3170−3178.

(11) See, K. C.; Feser, J. P.; Chen, C. E.; Majumdar, A.; Urban, J. J.; Segalman, R. A. *Nano Lett.* **2010**, *10*, 4664−4667.

(12) Ho, C. C.; Evans, J. W.; Wright, P. K. *J. Micromech. Microeng.* **2010**, *20*, 104009.

(13) Madan, D.; Chen, A.; Wright, P. K.; Evans, J. W. *J. Electron. Mater.* **2012**, *41*, 1481−1486.

(14) Chen, A.; Madan, D.; Koplow, M.; Wright, P. K.; Evans, J. W. *Proceedings of Power MEMS 2009*; Washington, D.C., Dec 1−4, 2009 ; Transducer Research Foundation: San Diego, CA, 2009

(15) Poudel, B.; Hao, Q.; Ma, Y.; Lan, Y.; Minnich, A.; Yu, B.; Yan, X.; Wang, D.; Muto, A.; Vashaee, D.; Chen, X.; Liu, J.; Dresselhaus, M. S.; Chen, G.; Ren, Z. *Science* **2008**, *320*, 634−638.

(16) Venkatasubramanian, R.; Siivola, E.; Colpitts, T. *Nature* **2001**, *413*, 597−602.

(17) Miller, G. R.; Li, C. Y. *J. Phys. Chem. Solids* **1965**, *26*, 173−177.

(18) Ha, H. P.; Cho, Y. W.; Byun, J. Y.; Shim, J. D. *J. Phys. Chem. Solids* **1994**, *55* (11), 1233−1238.

(19) Yim, W. M.; Rosi, F. D. *Solid-State Electron.* **1972**, *15* (10), 1121−1126.

(20) Yim, W.; Fitzke, E.; Rosi, F. D. *J. Mater. Sci.* **1966**, *1*, 52−65.

(21) Hyun, D. B.; Hwang, J. S.; Oh, T. S.; Shim, J. D. *J. Mater. Sci.* **2001**, *36*, 1285−1290.

(22) Madan, D.; Chen, A.; Wright, P. K.; Evans, J. W. *J. Appl. Phys.* **2011**, *109*, 034904.

(23) Madan, D.; Wang, Z.; Chen, A.; Juang, R. C.; Keist, J.; Wright, P. K.; Evans, J. W. *ACS Appl. Mater. Interfaces* **2012**, *4*, 6117−6125.

(24) Wang, Z.; Chen, A.; Winslow, R.; Madan, D.; Juang, R. C.; Evans, J. W.; Wright, P. K. *J. Micromech. Microeng.* **2012**, *22*, 094001.

(25) Lu, D.; Tong, Q. K.; Wong, C. P. *IEEE Trans. Electron. Packag. Manuf.* **1999**, *22*, 223−227.

(26) Lu, D.; Wong, C. P. *IEEE Trans. Electron. Packag. Manuf.* **2000**, *23*, 185−189.

(27) Lu, D.; Wong, C. P. *Inter. J. Adhes. Adhes.* **2000**, *20*, 189−202.

(28) Mclachlan, D. S.; Blaszkiewicz, M.; Newnham, R. E. *J. Am. Ceram. Soc.* **1990**, *73*, 2187−2203.

(29) Nan, C. W. *Prog. Mater. Sci.* **1993**, *37*, 1−116.

(30) Zhao, L. D.; Zhang, B. P.; Liu, W. S.; Zhang, H. L.; Li, J. F. *J. Alloys Compd.* **2009**, *467*, 91−97.

(31) Liu, Y. H.; Lin, Y. H.; Shi, Z.; Nan, C. W.; Shen, Z. J. *J. Am. Ceram. Soc.* **2005**, *88*, 1337−1342.

(32) Zhao, L. D.; Zhang, B. P.; Liu, W. S.; Zhang, H. L.; Li, J. F. *J. Appl. Phys.* **2009**, *105*, 023704.